AIAA JOURNAL
Vol. 59, No. 8, August 2021

Supersonic and Hypersonic Drag Coefficients for a Sphere

Eric Loth,* John Tyler Daspit,† and Michael Jeong†
University of Virginia, Charlottesville, Virginia 22903
and
Takayuki Nagata‡ and Taku Nonomura§
Tohoku University, Sendai Miyagi 980-8579, Japan

https://doi.org/10.2514/1.J060153

A comprehensive review of all relevant experimental data was completed, including recent data for the drag coefficient for a sphere in supersonic and hypersonic flows. The primary characterization parameter included the relative Mach, Knudsen, and Reynolds numbers based on the relative velocity, the sphere diameter, and other parameters. This review of data showed that the previously proposed nexus at a Reynolds number below 45 was not strictly met, and it instead included a weak transonic bump, which was identified numerically for the first time with the present simulations. New continuum-gas and rarefied-gas simulations were conducted and were combined with the expanded experimental dataset to improve the quantitative description of the drag coefficient in this region. The results indicated that a quasi nexus bridges the rarefaction regime and the compressible flow regimes. The comprehensive dataset was then used to develop new empirical models for the drag coefficient that showed improved robustness and accuracy as compared to previous models. These models are limited by the critical Reynolds number associated with boundary-layer transition on the sphere, which was found to increase substantially with the sphere Mach number.

Nomenclature

a	=	speed of sound in the gas
C	=	force coefficient
c	=	velocity coefficient
d	=	particle diameter
$\boldsymbol{F}$	=	force
f	=	Stokes correction factor
G	=	empirical parameter for subcritical Reynolds numbers
H	=	empirical parameter for Mach effects at nexus
J	=	empirical parameter for rarefaction effects
Kn	=	Knudsen number
l	=	length scale
M	=	Mach number
m	=	particle mass
n	=	number of particles in a group
Re	=	Reynolds number
r	=	radial coordinate
s	=	molecular speed ratio of the gas
$\boldsymbol{U}$	=	gas velocity around the particle surface
$\boldsymbol{u}$	=	gas velocity not influenced by the particle
$\boldsymbol{v}$	=	particle velocity
$\boldsymbol{w}$	=	particle velocity relative to the gas
x	=	axial coordinate
γ	=	specific heat ratio of gas
μ	=	dynamic viscosity of gas
ρ	=	density

Subscripts

accom	=	surface accommodation for noncontinuum effects
crit	=	critical value associated with drag crisis
D	=	drag
fm	=	free-molecular limit
g	=	gas characteristic
Kn	=	related to Knudsen number
m-m	=	mean free path between molecular collisions
o	=	incompressible continuum limit
p	=	particle characteristic
Re	=	related to Reynolds number
wall	=	at solid surface
θ	=	tangential momentum
@p	=	interpolated to particle centroid

I. Introduction

A WIDE range of aerospace applications includes spheres and spherical particles traveling at high speeds and/or in noncontinuum conditions. For example, hypersonic vehicles exposed to rain, ice crystals, and other meteorological particles can undergo significant surface damage due to the high-speed impact of these particles [1]. Rocket combustion chambers and flows with dusty detonations can also have particles at a high Mach number and/or a high Knudsen number [2,3]. Submicron particles can appear in supersonic boundary layers in various airbreathing propulsion systems [4]. Plasma sprays also often include supersonic flow regions with small melting metal particles for which two-way coupling effects can be important [5]. In such systems, the description of the drag is critical in terms for both particle trajectory and momentum coupling. Furthermore, a spherical shape is often a reasonable assumption. As such, there is significant interest to describe the drag coefficient of a sphere in high-speed relative flow conditions [6–12].

The quasi-steady drag force $\boldsymbol{F}_D$ of a sphere occurs in the opposite direction of the relative particle velocity $\boldsymbol{w}$, which is the difference between the particle velocity $\boldsymbol{v}$ and the gas velocity hypothetically interpolated to the particle center $\boldsymbol{u}_{@p}$. The influence of the relative velocity magnitude (i.e., $|\boldsymbol{w}|$) on the drag force for incompressible continuum flow depends on the particle Reynolds number Re_p. For supersonic and hypersonic flows past a particle, the additional effects of compressibility are characterized by the particle Mach number M_p, whereas the effects of rarefaction are characterized by the particle Knudsen number Kn_p. These three nondimensional

Received 15 October 2020; revision received 22 February 2021; accepted for publication 25 March 2021; published online Open Access 21 July 2021.

*Professor, Mechanical and Aerospace Engineering, 122 Engineer's Way. Fellow AIAA.
†Graduate Research Assistant, Mechanical and Aerospace Engineering, 122 Engineer's Way.
‡Postdoctoral Researcher, Department of Aerospace Engineering, 6-6-01 Aoba, Aramaki, Aoba-ku. Member AIAA.
§Associate Professor, Department of Aerospace Engineering, 6-6-01 Aoba, Aramaki, Aoba-ku. Senior Member AIAA.

parameters are related to the particle diameter d, the gas density ρ_g, the gas viscosity μ_g, the speed of sound a_g, the gas temperature T_g, the gas specific heat ratio γ, the gas constant $\mathcal{R}_g$, and the gas mean free path between molecular collisions l_{m-m} as follows:

$$\boldsymbol{w} \equiv \boldsymbol{v} - \boldsymbol{u}_{@p} \tag{1a}$$

$$Re_p \equiv \frac{\rho_g |\boldsymbol{w}| d}{\mu_g} \tag{1b}$$

$$M_p \equiv \frac{|\boldsymbol{w}|}{a_g} = \frac{|\boldsymbol{w}|}{\sqrt{\gamma \mathcal{R}_g T_g}} \tag{1c}$$

$$Kn_p \equiv \frac{l_{m-m}}{d} = \sqrt{\frac{\pi\gamma}{2}}\left(\frac{M_p}{Re_p}\right) \tag{1d}$$

The quasi-steady drag force $\boldsymbol{F}_D$ magnitude can also be expressed nondimensionally in terms of a drag coefficient C_D or in terms of the Stokes drag correction f as

$$\boldsymbol{F}_D = -\frac{1}{8}\pi\rho_g |\boldsymbol{w}| \boldsymbol{w} d^2 C_D = -3\pi d \mu_g f \boldsymbol{w} \tag{2a}$$

$$C_D = \frac{24}{Re_p} f \tag{2b}$$

The Stokes correction factor f is defined as the ratio of the drag coefficient at any Reynolds number relative to that for the creeping flow conditions for incompressible continuum flow for which $C_D = 24/Re_p$, i.e., $f = 1$ when $Re_p < 0.01$ and $Kn_p < 0.01$ [1,2,10]. In general, the drag coefficient can also be influenced by heat and mass transfer rates between the particle and the gas as well as the effects of particle shape, lift, added mass, and history forces (Refs. [13–20]). However, the present study focuses on nonspinning spherical particles in a uniform gas with quasi-steady adiabatic conditions. In particular, C_D (or f) are investigated in terms of Re_p, M_p, and Kn_p [where specifying two of these parameters specifies the third parameter according to Eq. (1d)]. The rarefaction and compressibility flow regimes can be characterized by the Mach and Knudsen numbers as indicated Tables 1 and 2, where the quantitative values are based on comprehensive review of available theory, data and models for the quasi-steady drag coefficient for spheres in a variety of conditions [6–12,21–53].

Of the three key parameters to be investigated, a Reynolds number has the strongest influence on the drag coefficient. The effects of Re_p for incompressible and continuum flow conditions ($M_p \to 0$ and $Kn_p \to 0$) on flow regimes and C_D are described in Table 1 and Fig. 1 [45,46], respectively. The most viscous condition ($Re_p \to 0$) is often referred to as the Stokes flow condition, where viscous and pressure stresses dominate the flowfield (so inertial effects can be neglected). The flowfield in this regime has a theoretical solution given by $f = 1$ per Eq. (2b). This is often referred to as the Stokes drag regime and results in a linear dependence of drag on the relative velocity in Eq. (2a). As the Reynolds number increases, the flow around a particle stays laminar, but convective effects lead to a reduced region of viscous effects, resulting in a boundary layer around a sphere once $Re_p \gg 1$. This boundary layer is generally attached for $Re_p < 22$, and then it has a steady separated region up to $Re_p < 130$. Figure 1 shows that the drag coefficient in this regime is larger than that predicted by Stokes drag ($C_D = 24/Re_p$, i.e., $f = 1$). At still higher Reynolds numbers, the laminar wake becomes unsteady and transitional (up to $Re_p < 1500$), and then fully turbulent ($Re_p > 1500$).

Table 1 Rarefaction flow regimes

Knudsen range	Flow physics
$Kn_p \le 0.01$	Continuum flow
$0.01 \le Kn_p \le 0.1$	Slip flow
$0.1 \le Kn_p \le 10$	Transition flow
$Kn_p \ge 10$	Free-molecular flow

Table 2 Compressibility flow regimes for a sphere

Mach range	Flow physics
$M_p \le 0.1$	Incompressible flow
$0.1 \le M_p \le 0.65$	Compressible subsonic flow
$0.65 \le M_p \le 1.2$	Transonic flow
$1.2 \le M_p < 5$	Supersonic flow
$M_p \ge 5$	Hypersonic flow

It can be seen that the drag coefficient is nearly constant for $1500 < Re_p < 250{,}000$. This is often described as the Newton regime corresponding to conditions for which the boundary layer on the sphere stays fully laminar until it separates, leading to a fully turbulent wake downstream. However, further increases in the Reynolds number are known to lead to a sudden drop in the drag coefficient. This is a result of the boundary layer transitioning to turbulent while it is still attached. This transition results in a fuller boundary layer that is more resistant to separation so that the separation point is moved downstream. As result, the turbulent wake zone is smaller such that the net pressure drag is reduced leading to the well-known "drag crisis." The Reynolds number when the attached boundary layer changes from laminar to turbulent has been called the "critical" Reynolds number $Re_{p,\text{crit}}$, and it can be defined as the Reynolds number when C_D first drops below 0.3 for incompressible continuum conditions. As such, the condition whereby the attached boundary layer on the sphere stays laminar up to separation is termed "subcritical" ($Re_p < 250{,}000$ for incompressible flow), whereas the condition where the boundary layer becomes transitional or turbulent before flow separation is termed the "supercritical" regime [1,11,16–18].

Measurements in the subcritical range have shown that C_D is approximately independent of Re_p (Fig. 1). This nearly constant value is called the "critical drag coefficient" $C_{D,\text{crit}}$ with a value of approximately 0.42. For the modeling of the drag coefficient from the Stokes regime to the critical Reynolds number, one may use the fit given by Clift and Gauvin [6] for $M_p \to 0$ and $Kn_p \to 0$:

$$C_{D,o} = \left[\frac{24}{Re_p}(1 + 0.15 Re_p^{0.687})\right] + \frac{0.42}{1 + (42{,}500/Re_p^{1.16})} \quad \text{for } Re_p < 2 \times 10^5 \quad \text{and} \quad Kn_p < 0.01 \tag{3}$$

Figure 1 shows that this widely used incompressible continuum model for drag is robust and accurate in this regime (to within 6% of experiments). In the following, this Clift–Gavin model is used as the basis for adding compressible and rarefaction flow effects for conditions up until the drag crisis.

When the Knudsen number increases as in Table 2, the flow around the particle can no longer be considered continuum. In this case, the molecules do not have a sufficiently high collision rate with the particle and each other, leading to a difference between the mean molecular velocity and the mean particle surface velocity, i.e., a partial-slip condition. This phenomenon is referred "accommodation," and the velocity difference results in a decrease in the drag relative to the continuum conditions. For slip flow, the noncontinuum effect is weak and can be molded with the Cunningham slip boundary condition [21]. Knudsen numbers much greater than unity are generally considered "free-molecular" flow conditions where the molecules impact and reflect from the particle surface, not with each other (theoretical analysis is again possible in this regime). The "transition" regime corresponds to Kn_p of order unity and is the most complex to theoretically analyze the Boltzmann equation; but, it can be

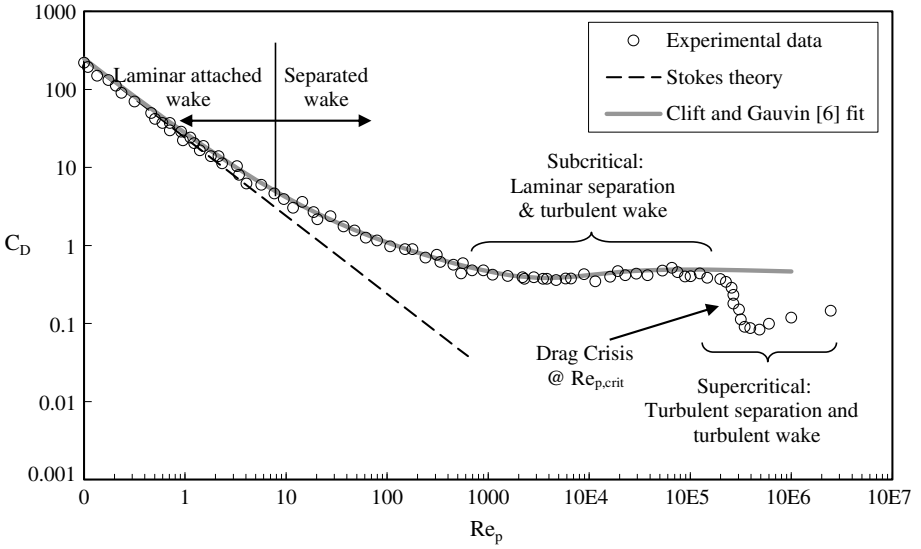

Fig. 1 Drag coefficient for a smooth solid sphere at various Reynolds numbers for incompressible continuum flow showing the model of Eq. (3) compared with experimental data reported by White [45] and Hoerner [46].

addressed numerically with the direct simulation Monte Carlo (DSMC) method [22,23].

Compressible flow features arise that modify the flowfield around the particle once the Mach number increases and the flow leads to transonic or supersonic regions, with observed examples of key flow features shown in Fig. 2 [47]. If one considers subcritical conditions for which a thin boundary layer is formed (e.g., $100 < Re_p < 1{,}000{,}000$), the flow will reach a sonic speed once the freestream Mach number is approximately 0.65. The sonic location first arises just above the boundary layer at an azimuthal position $\theta = 90$ deg away from the leading-edge stagnation point, which is consistent with potential flow theory. At still higher freestream speeds, the flow becomes transonic with the appearance of a lambda shock wave on the particle surface just upstream of $\theta = 90$ deg (Fig. 2a), with the flow becoming turbulent and separated at the leading leg of the lambda shock. Once the freestream flow is supersonic ($M_p > 1$), the lambda shock is replaced by a standoff normal shock in front of the sphere, which transits into an oblique shock further downstream (Fig. 2b). The flow separates at just upstream of $\theta = 90$ deg and leads to a weak recompression shock at this location. At still higher Mach numbers where the flow is hypersonic, the standoff shock becomes very close to the particle; it begins to interact with the boundary layer and to create a shock layer (Fig. 2c). Further downstream, and oblique shock with a very shallow angle forms while the flow separation shear layer becomes steadier (because it is more controlled by gas dynamics than turbulent instabilities). The result of this compressibility is a higher contribution of the pressure drag generally leading to a higher drag coefficient. In particular, high subcritical Reynolds numbers (e.g., $10{,}000 < Re_p < 1{,}000{,}000$) result in a rapid rise of C_D in the transonic regime with a maximum at $M_p \sim 1.4$, followed by a general reduction in the remaining supersonic regime of ($1.4 < M_p < 5$) and a relatively constant C_D for hypersonic conditions ($5 < M_p < 10$) that is still higher than that for incompressible flow [24].

The increase in a Mach number (compressibility) usually leads to an increase in the drag coefficient, whereas the increase in a Knudsen number (rarefaction) leads to a decrease in the drag coefficient. In particular, Loth [24] proposed that compressibility effects dominate for $Re_p > 45$ (whereby C_D increases with increasing M_p), whereas rarefaction effects dominate for $Re_p < 45$ (whereby C_D decreases with increasing M_p). In between, it was suggested that the competing effects cancel each other out, leading to a "nexus" condition, whereby a drag coefficient is independent of a Mach number (and a Knudsen number) for $Re = 45$, i.e.,

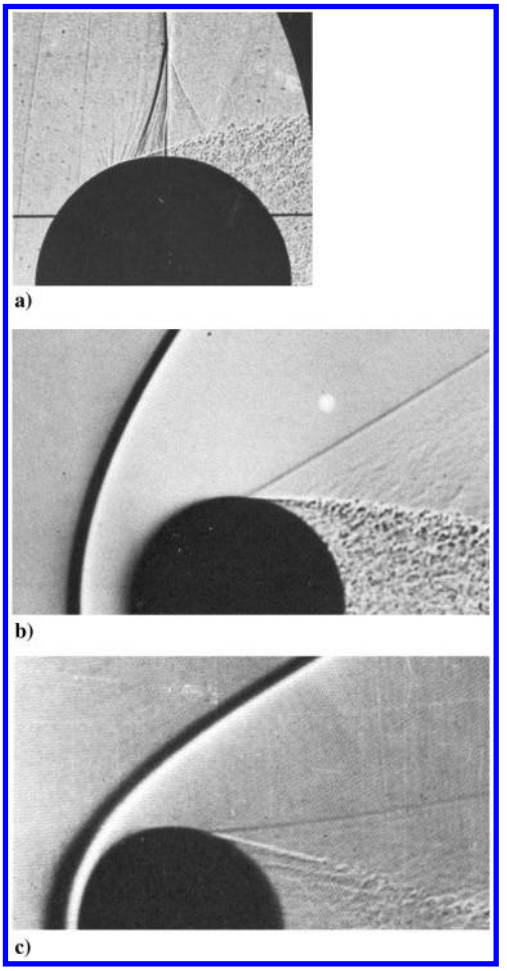

Fig. 2 Shadowgraphs and schlieren photographs [47] showing flow around spheres at subcritical Reynolds numbers for a) transonic conditions ($M_p \sim 0.8$), b) supersonic conditions ($M_p \sim 2.5$), and c) hypersonic conditions ($M_p \sim 7.6$).

$$C_D \sim 1.63 \quad \text{for } Re_p = 45 \text{ at all } M_p \quad \text{and} \quad Kn_p \tag{4}$$

Based on this nexus hypothesis, a rarefied model was developed for $Re < 45$ and a compressible model for $Re > 45$. Extensive review

of the data shows that this model was found to be superior in accuracy and robustness as compared to previous models.

Subsequent to the Loth model [24], Parmar et al. [25] developed a new model based on the dataset of Bailey and Hiatt [8] for transonic and some supersonic conditions, which provided improved accuracy when compared to this particular experimental dataset. However, the Parmar et al. model is limited to $M_p < 1.75$ and $Kn_p < 0.01$ (no hypersonic conditions) and employs a nonlinear interpolation with 50 empirically determined coefficients. Furthermore, it was not evaluated against much of the previous experimental data reviewed for the Loth model.

Based on the preceding, there is a motivation to develop a drag model for spheres that is robust for a large range of Mach numbers and should consider all available experimental data, including more recent experiments and simulations of particle drag in the supersonic and rarefied conditions. Ideally, such a model would be based on a modest number of empirical coefficients and would provide improved accuracy. Furthermore, such a model should consider combinations of Mach and Knudsen numbers where no previous data exist. In particular, there are data in the nexus region of Eq. (4) based on experimental data with substantial scatter, and there have not been high-fidelity simulations of the drag near the nexus for the verification of the accuracy of the nexus assumption. Therefore, there is a clear need for additional data into this region to better understand the trends where effects of both compressibility and rarefaction strongly compete.

The objectives of the current study are threefold. The first objective is to conduct a comprehensive data review that not only includes the previous experimental data used by Loth [24] and Parmar et al. [25] but also incorporates more recent experimental and computational data that have since become available. A second objective is to conduct new simulations to add additional detail to more accurately describe the combined impact of compressibility and rarefaction in the vicinity of the hypothetical nexus condition. The third objective is to evaluate the previous drag models relative to a full comprehensive review of previous data and new simulation data in order to assess their accuracy and robustness, as well as to allow the development of a new set of models that could be even more robust and accurate. To the authors' knowledge, this is the first such published study to address these three objectives.

II. Methodology

A. Comprehensive Data Review

A detailed survey of all experimental data was conducted. This included the data assembled by Loth [24] and Parmar et al. [25], resulting in the first study to combine these two experimental datasets. However, a key objective of the present study was to compile all available high-fidelity data obtained by experiments and simulations. Therefore, measurements of high-speed drag coefficients were included from several additional sources, including Jacobs [26], Roos and Willmarth [27], Short [28], Spearman and Braswell [29], and Theofanous et al. [30]. As a result, the experimental data represent the most comprehensive review of supersonic and hypersonic sphere drag data. In addition, recent direct numerical simulations of continuum flow by Nagata et al. [31,32] were also included. However, there is a scarcity of high-confidence data in the vicinity of the proposed nexus (Re_p of around 45 and $M_p > 0.6$). Therefore, additional simulations for flow over a sphere were conducted using the methods described in the following, and drag coefficients were obtained in the regime where both rarefaction and compressibility are important.

B. DSMC Computational Approach

DSMC was used to provide the drag for conditions with significant rarefaction ($Kn > 0.1$). The simulations were completed using an open-source DSMC code developed by Sandia National Laboratories: SPARTA [33]. Herein, only laminar steady flows are considered, which limits the Reynolds number to be less than 45 and allows axisymmetric solutions.

The axisymmetric domain was defined by a radial coordinate r and a streamwise coordinate x, as shown in Fig. 3a. An inflow boundary was set at 10 diameters upstream ($x = -10d$), whereas specular reflection and outflow boundaries were set at the outer radial boundary ($r = 10d$) and at the downstream boundary ($x = 10d$), respectively. A periodic boundary condition was imposed in the azimuthal direction, consistent with axisymmetric boundary conditions. The inflow temperature was set at 293 K, and the isothermal boundary condition with 293 K was imposed on the surface of the sphere was set as at 293 K. For velocity, a Maxwell boundary condition was applied on the surface of the sphere. The accommodation coefficient c_{accom} is the fraction of molecules that undergo a diffuse reflection upon impacting the particle surface, whereas the remaining fraction undergoes specular reflection. In the DSMC predictions, $c_{\text{accom}} = 0.9$: a value that is consistent with a smooth surface and experimental results [24].

The baseline grid used two different resolutions, as shown in Fig. 3b, where the near-field grid spacing in all directions was one-fourth that of the far-field grid spacing. The grid width and time step were set to be less than the mean free path and the mean collision time, respectively. The quantities of the flowfield were sampled as the averaged values during 5000 steps to get one averaged flowfield. After the flowfield becomes statistically steady, the averaged flowfield was computed again using more than 20 averaged flowfields. Examples of the velocity and number-density distributions are shown in Fig. 4. The drag coefficient was calculated using flow data after the flowfield achieved a statistically steady state, and grid and time-step resolution studies indicated that the drag values converged to within 1% for all simulations.

C. Navier–Stokes Computational Approach

To consider conditions with weak or no rarefaction, additional simulations were conducted with the full Navier–Stokes equations, with all viscous effects fully resolved. This approach is often referred to as Direct Numerical Simulation (DNS) and can be used to treat flows in the laminar, transitional, or turbulent regime. In the

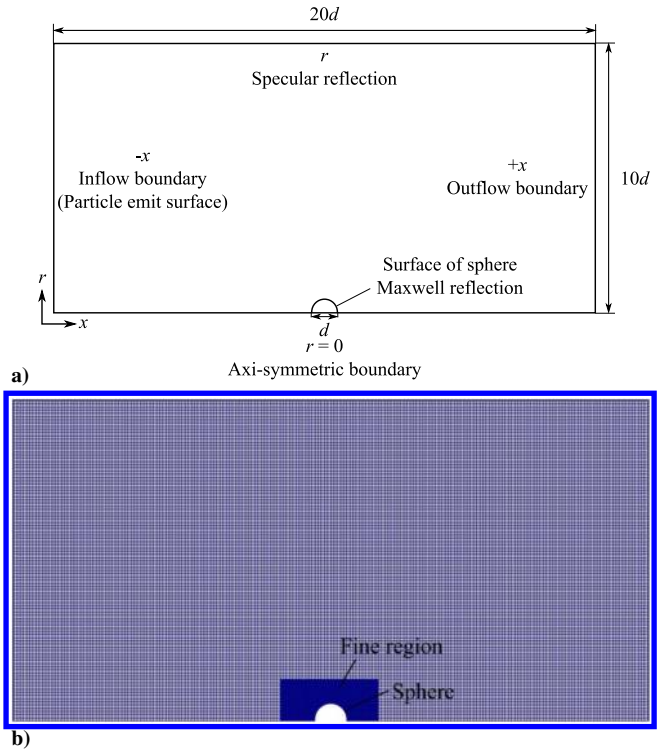

Fig. 3 DSMC flow plane for the streamwise direction x and radial direction r showing a) boundary conditions for this plane (periodic boundary conditions used in the azimuthal direction) and b) computational grid showing course and fine grid regions.

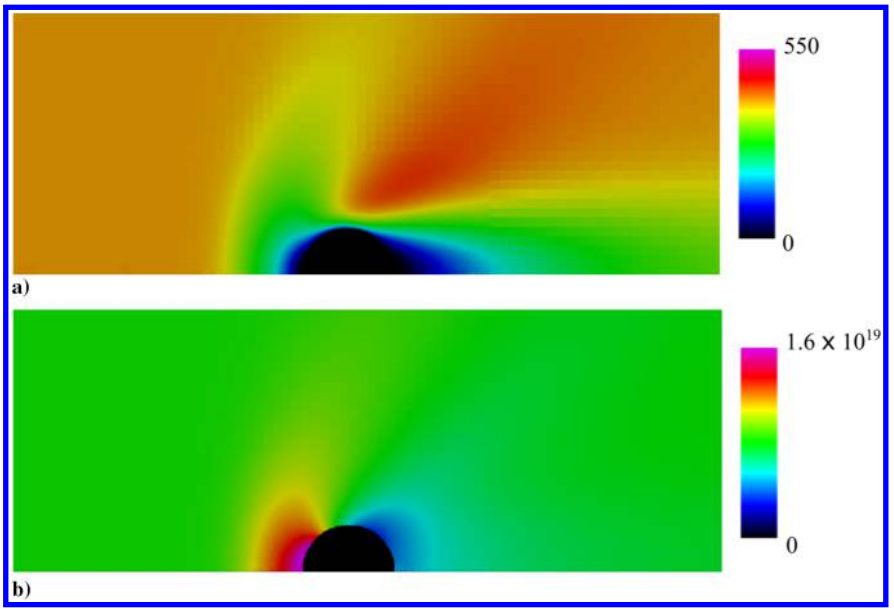

Fig. 4 Example DSMC results for $Re_p = 45$ and $Kn_p = 0.242$ ($M_p = 1.2$) in the streamwise–radial plane showing contour distributions of a) velocity relative to the sphere (in meters per second) and b) number density (per cubic meter).

continuum regime ($Kn_p < 0.01$), these equations can be employed with a no-slip condition. For weak rarefaction conditions ($0.01 < Kn_p < 0.1$), the surface velocity conditions can be treated using a Maxwell slip relationship [34]. In particular, the difference between the local wall tangential velocity U_{wall} and that of the fluid U for a spherical coordinate system is related to the distance above the surface ($r - r_p$), the radial velocity gradient, and the tangential momentum coefficient c_θ as

$$U_{\text{wall}} = U + \frac{c_\theta d}{r - r_p} Kn_p \frac{\partial U}{\partial r} \tag{5a}$$

$$c_\theta = \frac{2 - c_{\text{accom}}}{c_{\text{accom}}} \tag{5b}$$

For weak rarefaction, the focus was on laminar steady flows with $Re_p < 200$ for subsonic conditions and $Re_p < 300$ for transonic conditions to ensure steady axisymmetric conditions.

Adiabatic conditions were also assumed, which is consistent with a particle temperature equal to the surrounding gas temperature. The particle temperature can be different from the ambient temperature if the particle is undergoing rapid heating or cooling (e.g., due to injection conditions, shock passage, etc.). However, the effect of temperature difference on drag is generally small for the Reynolds numbers simulated based on experimental data [7,8].

Discretized governing equations were solved by an in-house computational code with high-order schemes, boundary conditions, and computational grids where the computational code has been validated in detail for drag over spheres [31,32]. The convection terms were evaluated by the sixth-order adaptive central and upwind weighted essentially nonoscillatory scheme WENOCU6-FP of Nonomura et al. [35], but the central difference component was replaced by the splitting type proposed by Pirozzoli [36] in order to stabilize the calculation. The viscous terms were evaluated by the sixth-order central difference method. The time integration is conducted by the third-order total variation diminishing Runge–Kutta method proposed by Gottlieb and Shu [37].

III. Results

A. Quasi Nexus

The previously proposed nexus condition suggested that the drag coefficient was independent of a Mach number for $Re_p = 45$ [per Eq. (4)]. This trend is consistent with results that show that higher Reynolds numbers generally yield an increase in C_D as M_p increases (due to compressibility effects that create a higher-pressure drag over the surface), whereas lower Reynolds numbers generally lead to a decrease in C_D as M_p increases (due to rarefaction effects that result in a slip velocity on the surface).

To investigate the validity of the nexus, all available data including new simulations conducted for this study were collected for a range of Mach numbers at $Re_p \sim 45$, as shown in Fig. 5 [48,49]. Although there is considerable spread and uncertainty in the experimental data (gray and black filled symbols), the computational results (open symbols) clearly indicate a transonic bump that is inconsistent with the Loth model [24], which is shown as a dashed line. In particular, the drag coefficient increases in the subsonic range from the incompressible value of 1.63 for $M_p < 0.1$ to $C_D \sim 2$ at $M_p \sim 1$. For supersonic Mach numbers, the drag coefficient decreases and then returns approximately to the incompressible values of 1.63 for hypersonic conditions ($M_p > 5$). These results indicate that the nexus proposed in Eq. (4) is not strictly realized. Instead, a more accurate description for Re_p near 45 is a "quasi nexus" where the influences of a Mach number are minimized but still significant. In particular, the expected continuum flow increases in C_D due to compression tended to be mostly (but not completely) canceled by the decreases in C_D due to rarefaction in the vicinity of Re_p of 45. In particular, the present simulations found that the wave drag effects tend to increase the pressure on the fore side of the sphere (thereby increasing drag), whereas rarefaction effects reduce the velocity gradient on the surface due to partial slip (thereby decreasing drag). This is an important aspect in constructing empirical models for the drag coefficient.

This figure also shows the empirical models for the compressible regime and for the rarefied regimes, which are seen to be well bridged at this Reynolds number (i.e., within 1% of each other) and reasonably reflect the transonic bump trends described earlier in this paper. These two empirical models are discussed in the following two sections. However, there is a wide variation in data at this particular Reynolds number. Experimental measurements are notoriously hard to obtain with high accuracy because the entire flow can be highly unstable due to the shock movement interactions with the boundary layer. In particular, small surface variations or upstream unsteadiness can cause significant shock movement, thereby changing the surface pressure over the sphere. In addition, transonic flows are highly sensitive to flow blockage effects, with the present simulations indicating a boundary condition of 10 diameters (Fig. 3) as being critical for this condition, which is more than any other Mach number conditions. This may be one of the reasons that there have been no

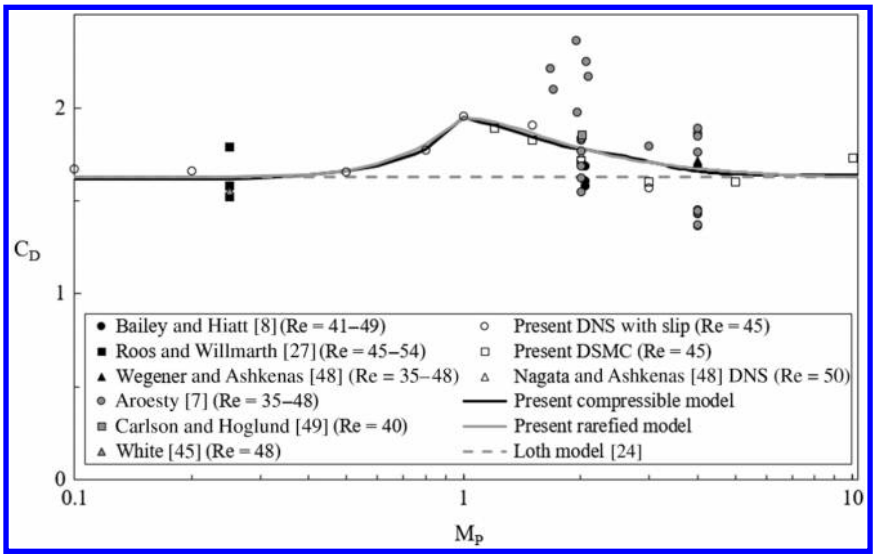

Fig. 5 Drag coefficient as a function of Mach number near nexus conditions ($Re_p \sim 45$) including experimental results [7,8,27,45,48,49] recent simulations [31], present DNS and DSMC simulations, nexus model [24] [Eq. (4)], as well as present models for the compressible flow regime [Eqs. (6–8)] and the rarefied regime [Eqs. (9–15)].

previous detailed simulations for this condition before the present work. As such, further work is needed to improve the understanding and modeling of the quasi nexus.

B. Compression-Dominated Regime

The influence of a Mach number on the drag coefficient is well known at high Reynolds numbers in the subcritical regime, as discussed in the Introduction (Sec. I). As expected, the compression-dominated regime generally yields increased drag as the Mach number increases, which then settles to a near-constant value. Based on Refs. [24] and [25], the effects of compressibility at high Reynolds numbers (e.g., $10,000 < Re_p < 1,000,000$) can be expressed in terms of a drag coefficient ratio defined as

$$C_M \equiv \frac{C_{D,\text{crit}}}{C_{D,\text{crit},M=0}} = \frac{C_{D,\text{crit}}}{0.42} \tag{6}$$

This expression uses a baseline (incompressible) critical drag coefficient of 0.42, which is consistent with the value at high subcritical Reynolds numbers as shown in Fig. 1. However, the current study sought to review all available experimental data and to accurately describe the influence of M_p on C_M. This updated collection of data is shown in Fig. 6. It can be seen that the models of Loth [24] and Parmar et al. [25] reasonably captured the trends in C_M, but the Parmar et al. model tends to overpredict at lower Mach numbers. It should be noted that the previous models were only based on the data reported by Hoerner [46]. Based on this updated collection of all data available (which differs slightly), a new model is proposed for C_M as

$$C_M = 1.65 + 0.65\tanh(4M_p - 3.4) \quad \text{for } M_p < 1.5 \tag{7a}$$

$$C_M = 2.18 - 0.13\tanh(0.9M_p - 2.7) \quad \text{for } M_p > 1.5 \tag{7b}$$

This new model is simpler than that proposed by Loth [24] and is the most accurate of the models shown in Fig. 6.

To investigate the influence of Mach number between the quasi-nexus point (Fig. 5) and the high-Re_p regime (Fig. 6), data were collected (including present simulations) as a function of a Reynolds number for a set of Mach numbers as shown in Fig. 7 [46–52]. For the nearly incompressible case of $M_p \sim 0.2$ (Fig. 7a), there is the local minimum of C_D in the range of 1000 to 10,000 beyond which the drag

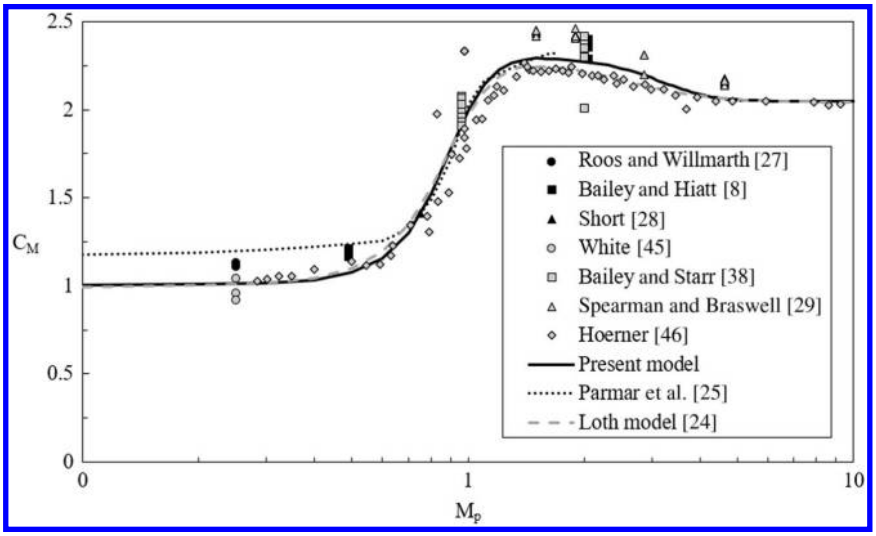

Fig. 6 Drag coefficient as a function of Mach number at subcritical conditions in the Newton-based drag regime ($10,000 < Re_p < 1,000,000$) including experimental results [8,24,25,27–29,38,45,46], the present compressible flow model [Eqs. (6–8)] and previous models.

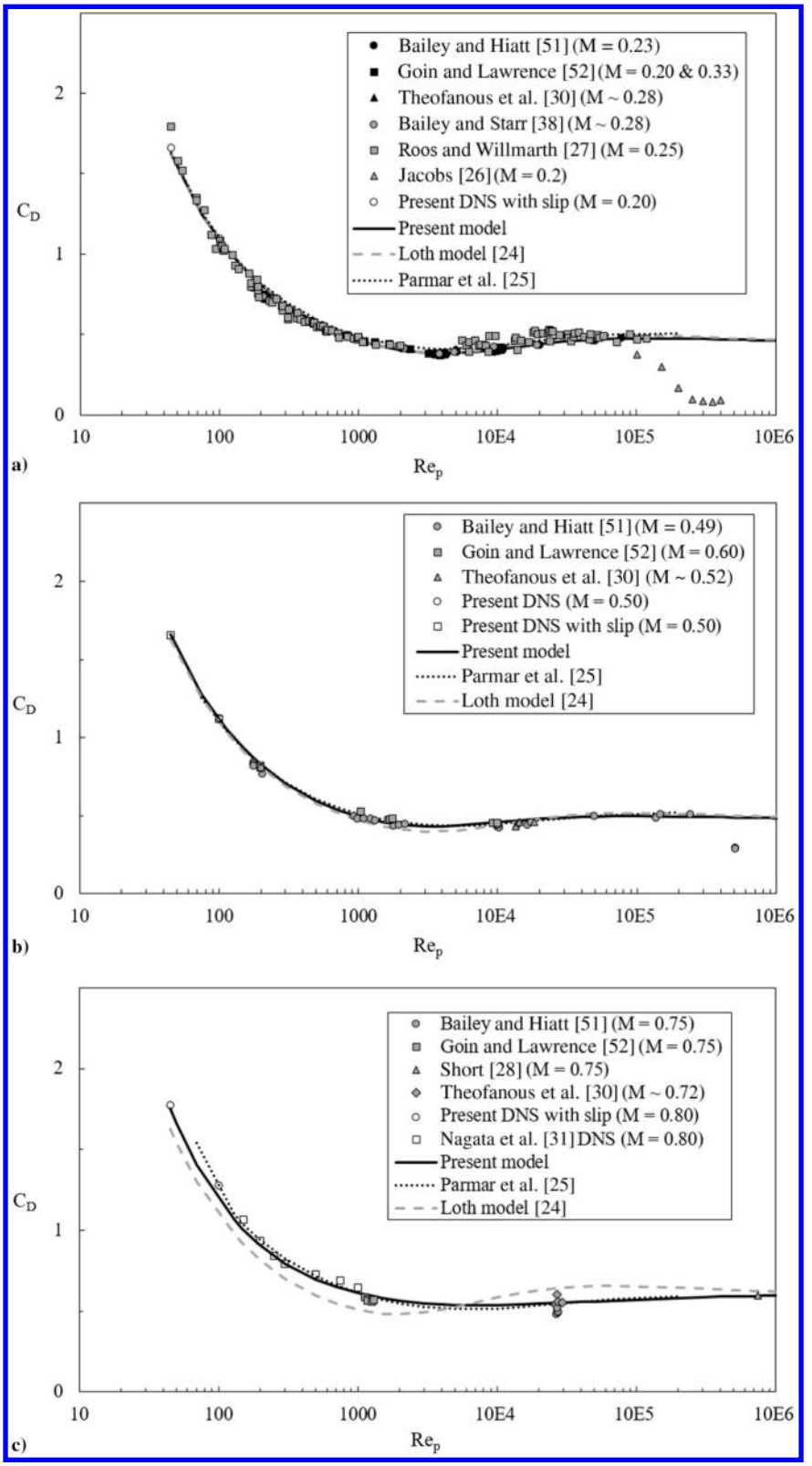

Fig. 7 Drag coefficient in compressible regime ($Re_p > 45$) as a function of Reynolds number based on experimental and computational data [7,8,26–32,38,46–52] as well as present simulations and empirical models including the present compressible flow model [Eqs. (6–8)] for a) $M_p \sim 0.25$, b) $M_p \sim 0.5$, c) $M_p \sim 0.75$, d) $M_p \sim 0.83$, e) $M_p \sim 1$, f) $M_p \sim 1.5$, g) $M_p \sim 2$, h) $M_p \sim 4$, i) $M_p \sim 5.5$, and j) $M_p \sim 10$.

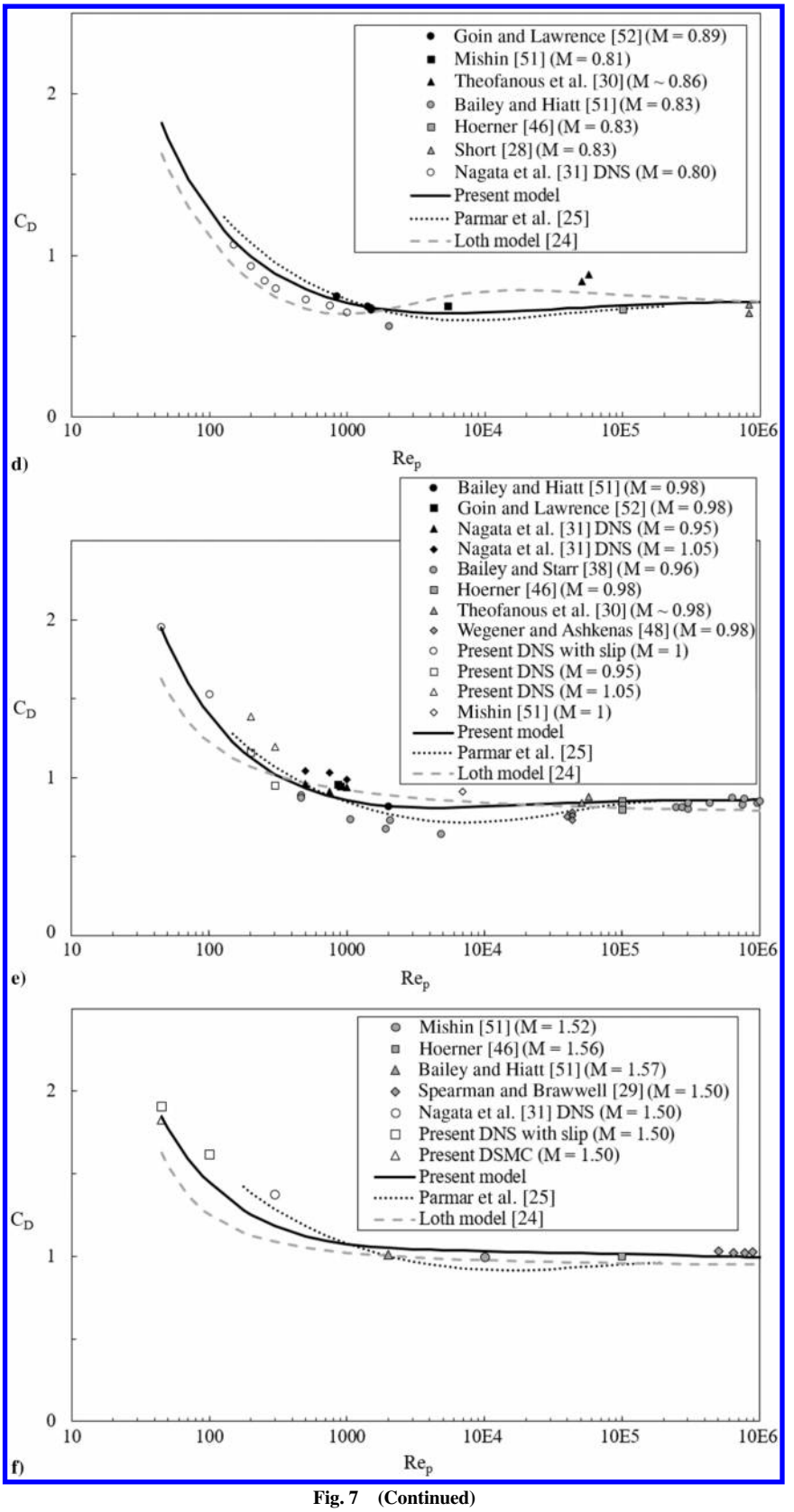

Fig. 7 (Continued)

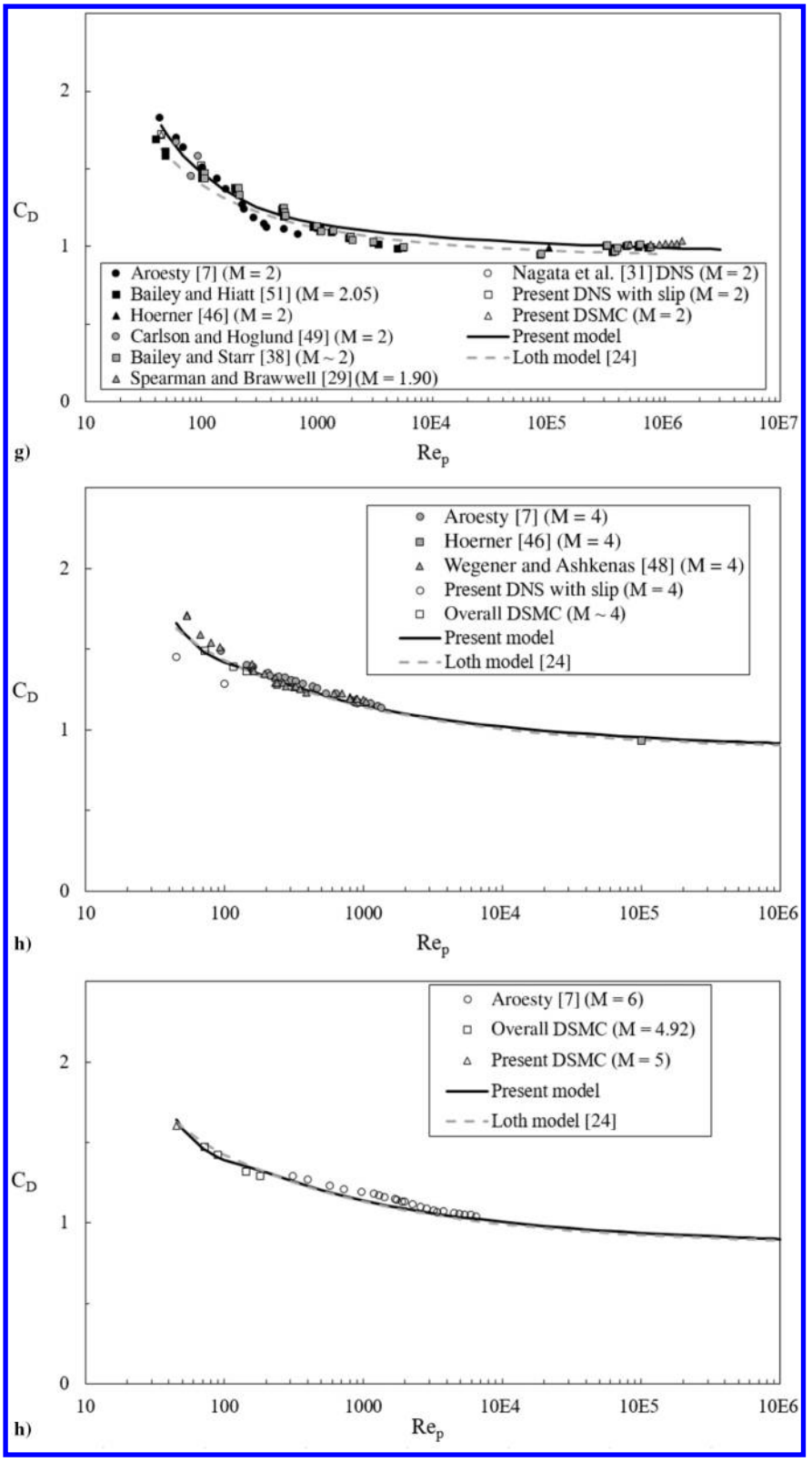

Fig. 7 (Continued)

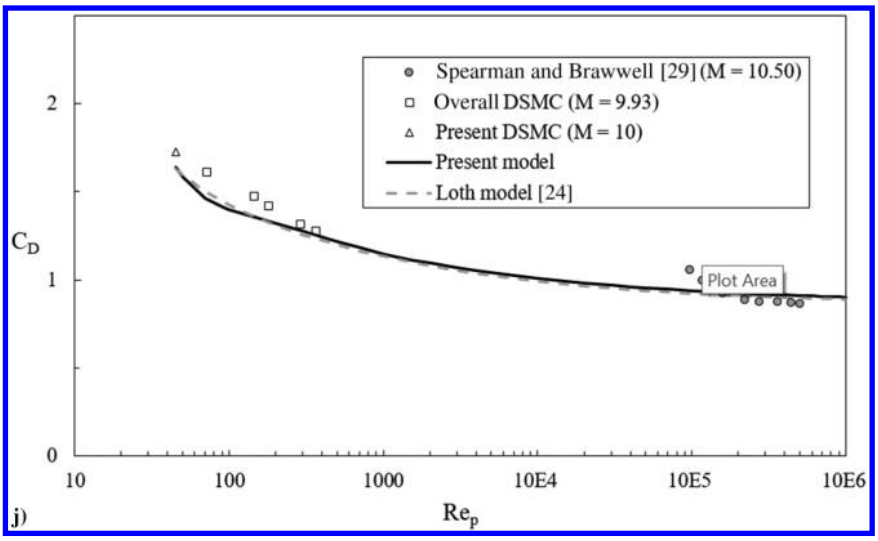

Fig. 7 (Continued)

rises to its critical value for the Newton regime of 0.42 (as seen in Fig. 1). At even higher Reynolds numbers, the drag drops again due to transition of the attached boundary layer from laminar to turbulent. The associated drag crisis is shown to occur at $Re_{p,\text{crit}} \sim 150{,}000$ in this case. As the Mach number increases to transonic conditions (Figs. 7b–7e), the drag coefficient is elevated at all Reynolds numbers. In addition, the local minimum of the C_D in the range of 1000 to 10,000 is eliminated and the drag crisis is delayed at higher Reynolds numbers ($Re_{p,\text{crit}} > 800{,}000$ for $M_p > 0.75$). As the Mach number becomes supersonic and hypersonic (Figs. 7f–7j), the drag coefficient is seen to continually reduce as the Reynolds number increases. In addition, the drag crisis continues to be delayed (e.g., $Re_{p,\text{crit}} > 1{,}500{,}000$ for $M_p > 2$) based on experimental results [38]. This is attributed to the increasing stability of the boundary layer on the sphere surface as the Mach number rises, as has been demonstrated experimentally and theoretically for flat-plate boundary layers [39,40]. Although there are insufficient experimental data to accurately provide a model of $Re_{p,\text{crit}}$ for various M_p, this influence should be kept in mind when employing high-speed drag coefficient models.

To describe the compressible flow trends in the drag coefficient based on all the available experiments and simulations with $Re_p > 45$, a modified Clift–Gauvin drag expression was developed with Eq. (7) as

$$C_D = \frac{24}{Re_p}(1 + 0.15Re_p^{0.687})H_M + \frac{0.42C_M}{1 + (42,500/Re_p^{1.16C_M}) + (G_M/Re_p^{0.5})} \quad \text{for } 45 < Re_p < Re_{p,\text{crit}} \tag{8a}$$

$$G_M = 166M_p^3 + 3.29M_p^2 - 10.9M_p + 20 \quad \text{for } M_p < 0.8 \tag{8b}$$

$$G_M = 5 + 40M_p^{-3} \quad \text{for } M_p > 0.8 \tag{8c}$$

$$H_M = 0.0239M_p^3 + 0.212M_p^2 - 0.074M_p + 1 \quad \text{for } M_p < 1 \tag{8d}$$

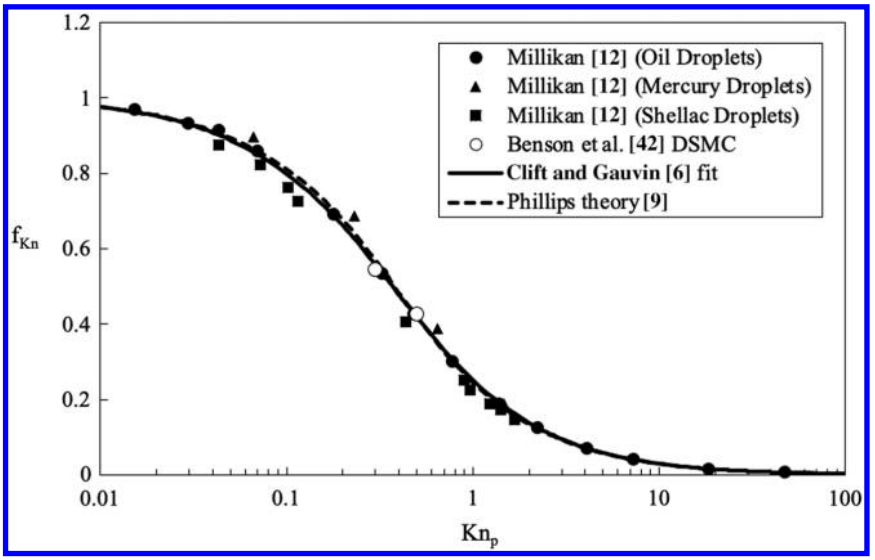

Fig. 8 Stokes drag correction as a function of Knudsen number for experimental and computational data [12,42] along with the Clift and Gauvin model of Eq. (10).

$$H_M = 0.93 + \frac{1}{3.5 + M_p^5} \quad \text{for } M_p > 1 \tag{8e}$$

Figures 7a–7j illustrate that the present model is more accurate and robust for supersonic and hypersonic conditions than the previous models of Loth [24] and Parmar et al. [25]. Furthermore, the present formulations of G_M and H_M are simpler in form than those previously proposed by Loth [24]. The quantitative differences between the various model predictions compared to the data from experiments and high-fidelity numerical simulations are discussed later.

C. Rarefaction-Dominated Regime

The effect of rarefaction becomes important for finite Knudsen numbers, and this effect tends to dominate the drag coefficient trends of $Re_p < 45$. When the flow is in continuum ($Kn_p \to 0$), the drag force for a spherical particle given by Eq. (3) is reasonable for $Re_p < 45$. For finite Knudsen numbers in creeping flow ($Re_p \to 0$), the Cunningham correction factor is defined as

$$f_{Kn} \equiv \frac{F_{D,Re\to 0}}{3\pi\mu_g d} \tag{9}$$

For a small Mach number ($M_p \ll 1$), Clift and Gauvin [6] developed a simple empirical model that is consistent with $c_\theta \approx 1.22$ and the approximate theory of Phillips [9] (which bridged the theoretical result by Basset [10] for $Kn_p \ll 1$ and that of Epstein [11] for $Kn_p 1$) as

$$f_{Kn} = \frac{1}{1 + Kn_p[2.514 + 0.8\exp(-0.55/Kn_p)]} \tag{10}$$

As shown in Fig. 8, this model agrees with the theoretical results and experiments of Milliken [12,41] and the DSMC of Benson et al. [42] that showed a decrease in drag with increasing Kn_p. To extend Eq. (10) to include finite Reynolds numbers in the rarefaction-dominated regime ($Re_p < 45$), the Knudsen number effect can be modified to include a Schiller–Naumann correction [24] as

$$C_{D,Kn,Re} = \frac{24}{Re_p}(1 + 0.15Re_p^{0.687})f_{Kn} \tag{11}$$

It should be noted that Eq. (11) is limited to weak compressibility effects ($M_p \ll 1$).

To incorporate rarefied conditions with high-Mach-number condition effects, one may instead consider the free-molecular limit, which can be characterized by the molecular speed ratio s defined by the Mach number and specific heat ratio as

$$s \equiv M_p\sqrt{\gamma/2} \tag{12}$$

Assuming equal tangential and normal accommodation coefficients and equal particle and gas temperatures, the free-molecular compressibility limit for $s > 1$ as obtained by Stalder and Zuric [43] and Schaff and Chambré [44] is

$$C_{D,fm} = \frac{(1+2s^2)\exp(-s^2)}{s^3\sqrt{\pi}} + \frac{(4s^4+4s^2-1)\mathrm{erf}(s)}{2s^4} + \frac{2}{3s}\sqrt{\pi} \tag{13}$$

In the limit of $s \to \infty$, $C_{D,fm} \to 2$, which can be taken as the lower limit of the rarefied drag coefficient for $Re_p \ll 1$. Herein, this free-molecular limit can be empirically corrected for finite Reynolds numbers as

$$C_{D,fm,Re} = \frac{C_{D,fm}}{1 + [(C_{D,fm}/J_M) - 1]\sqrt{(Re_p/45)}} \tag{14a}$$

$$J_M = \begin{cases} 2.26 - \frac{0.1}{M_p} + \frac{0.14}{M_p^3} & \text{for } M_p \le 1 \\ 1.6 + \frac{0.25}{M_p} + \frac{0.11}{M_p^2} + \frac{0.44}{M_p^3} & \text{for } M_p > 1 \end{cases} \tag{14b}$$

Compared to those previously proposed by Loth [24], the present forms of $C_{D,fm,Re}$ and J_M are simplified via the assumption of equal gas and particle temperatures but also fix a typo for $C_{D,fm,Re}$ that should have included the last specular reflection term in Eq. (13).

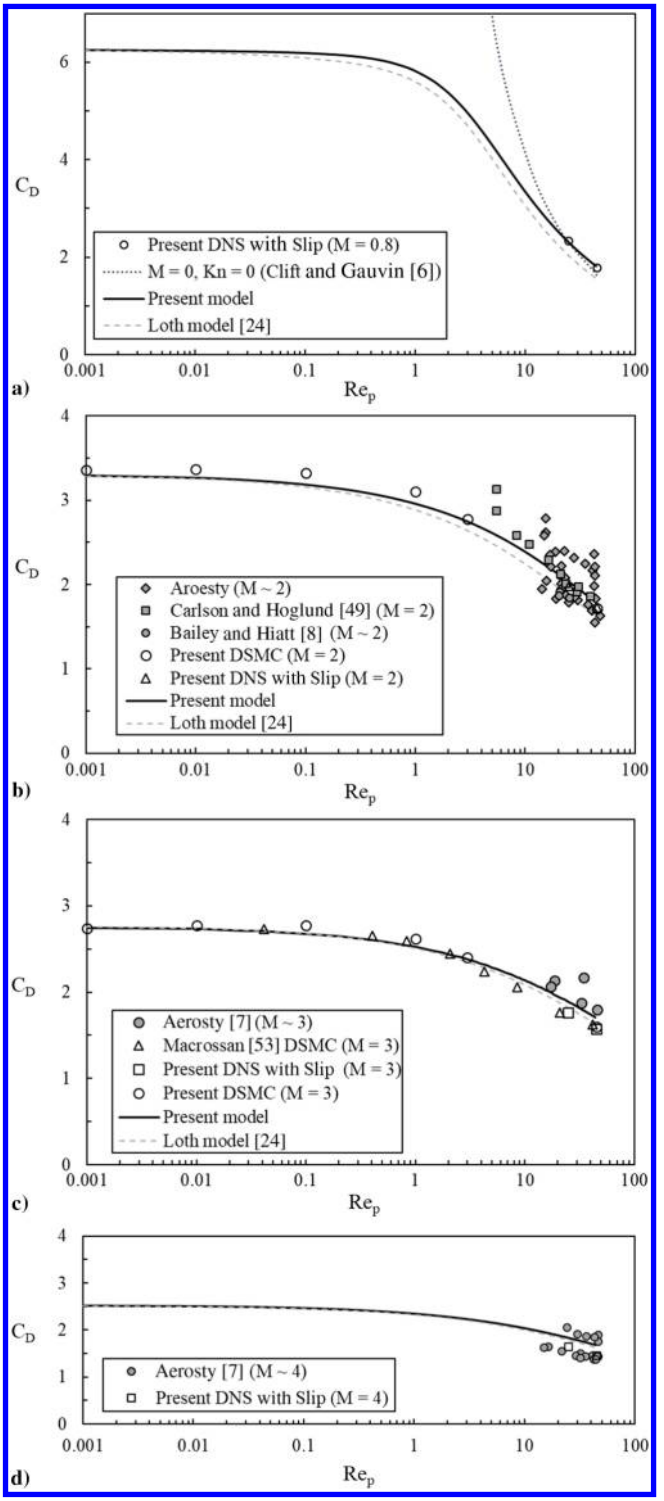

Fig. 9 Drag coefficient in rarefaction regime ($Re_p < 45$) as a function of Reynolds number based on previous data [7,8,49,53], as well as present simulations and empirical models [Eqs. (9–15)] for a) $M_p \sim 0.8$, b) $M_p \sim 2$, c) $M_p \sim 3$, d) $M_p \sim 4$, e) $M_p \sim 5$, and f) $M_p \sim 10$.

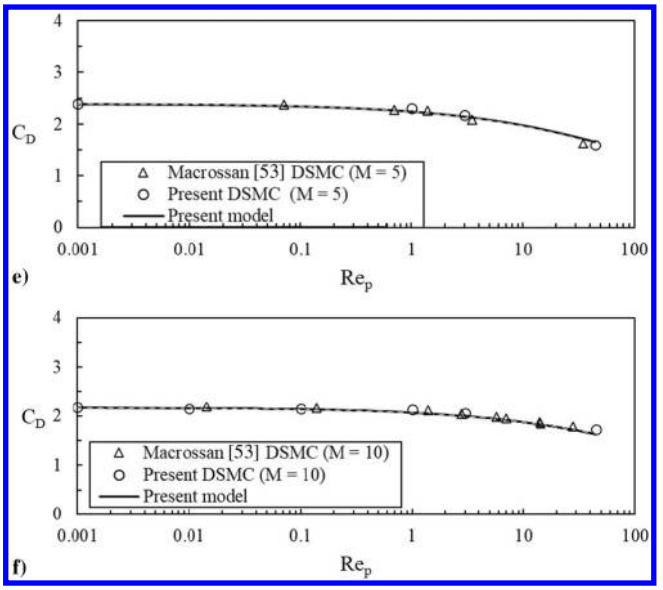

Fig. 9 (Continued)

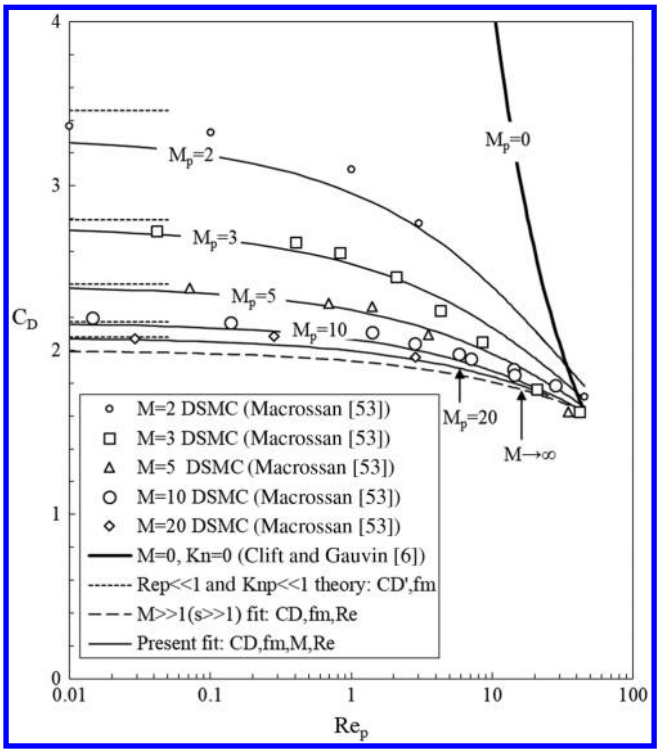

Fig. 10 Drag coefficient (C_D) variations in rarefaction regime ($Re_p < 45$) showing limits for incompressible continuum flow (thick solid line), free-molecular flow (long dash line), and hypersonic creeping flow (short dashed line), along with typical DSMC results [53].

Finally, the weak Mach-number-limit of Eq. (11) can be blended with the high-Mach-number limit of Eq. (14) in the rarefaction-dominated regime using the empirical expression of Loth [24]:

$$C_D = \frac{C_{D,Kn,Re}}{1 + M_p^4} + \frac{M_p^4 C_{D,fm,Re}}{1 + M_p^4} \quad \text{for } Re_p \leq 45 \qquad (15)$$

The preceding set of equations integrates the combined influence of the Reynolds, Mach, and Knudsen numbers for the rarefaction-dominated regime and are simpler in form than the model of Loth [24].

Figures 9 and 10 show the overall behavior for the rarefaction regime with an increasing Mach number. In general, increasing rarefaction results in a decreasing drag coefficient, which is consistent with increasing the slip conditions on the particle surface. In addition, it can be seen that the drag coefficient tends to a constant value for $Re_p \ll 1$ for all the supersonic and hypersonic conditions that were evaluated (Figs. 9a–9g) [53]. For the hypersonic conditions, this tendency yields $C_D \to 2$ as $Re_p \to 0$, which is consistent with the free-molecular limit (shown by the dashed lines in Fig. 10).

In general, the present empirical model given by Eqs. (10–15) predicts all the trends observed by the experiments and simulations, including the new simulations conducted for this study. The model predictions are effectively the same for hypersonic flow ($M_p > 5$) as those of Loth [24] but are more accurate for subsonic and supersonic flows. In general, the model predicts the limiting value of a drag coefficient for $Re_p \ll 1$ observed in the data for supersonic and hypersonic conditions (Fig. 10). However, it should be noted that the model also predicts a limiting behavior for $M_p = 0.8$, as shown in Fig. 9a ($C_D \to 6.2$ as $Re_p \to 0$), but there are no experiments or simulations that confirm this result. As a result, it is recommended that simulations and experiments should be conducted to better characterize the influence of Mach number on the drag coefficient in the subsonic limit of creeping flow at rarefied conditions. However, the current models accurately and robustly predict all the trends and values given by the available data in this comprehensive review. The overall trends are shown in Fig. 11, including the quais-nexus.

D. Accuracy Assessment of Models and Overall Drag Behavior

Figures 6–10 show that the present model for the drag coefficient of supersonic and hypersonic flows past spheres is generally accurate and robust in terms of predictive performance for a wide range of Mach, Knudsen, and Reynolds numbers. To quantitatively assess the accuracy of the present model and those of Loth [24] and Parmar et al. [25], a detailed error analysis relative to all the experimental and computational results presented in this paper was completed. Since the error was based on the difference between each data point presented, the error included uncertainty associated with the data itself. For example, the significant variation in the experimental data at transonic conditions (e.g., Fig. 6) meant that there was a lower bound on the accuracy of any empirical model that could be proposed.

The net errors for three Mach regimes are shown in Table 3, where it can be seen that the present model is approximately twice as accurate as either the Loth model [24] or the Parmar et al. model [25] for moderate Mach numbers ($M_p < 2$) in compressible-dominated flow and is generally more accurate than the Loth model [24] for both higher Mach numbers ($M_p > 2$) and for rarefied conditions ($Re_p < 45$). Since those two previous models were found to be superior to others presented previously [39,40], the present model appears to be the most accurate and robust empirical model yet developed for compressible-dominated and rarefied-dominated conditions.

IV. Conclusions

A comprehensive review of all relevant experimental data was completed to characterize the influence of relative Mach, Knudsen, and Reynolds numbers on the drag coefficient of a sphere

Table 3 Average root-mean-square difference for drag models based on all available data[a]

Model	Rarefied flow ($Re_p < 45$), %	Moderate Mach ($Re_p \geq 45$, $M < 2$), %	High Mach ($Re_p \geq 45$, $M \geq 2$), %
Loth [24]	10.7	9.9	3.6
Parmar [25]	N/A	10.0	N/A
Present model	6.1	4.9	3.4

[a]N/A denotes "not applicable."

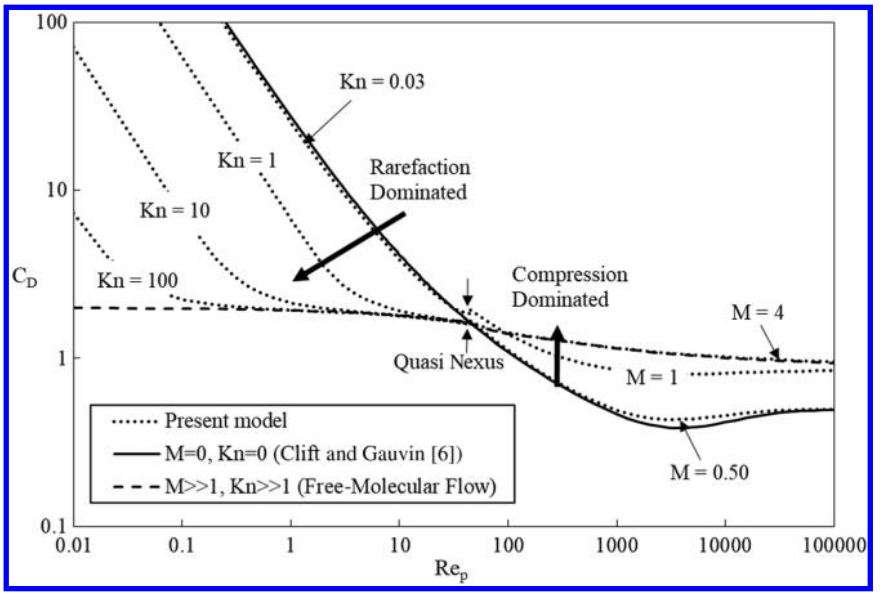

Fig. 11 Rarefaction and compression effects on drag of a spherical particle based on updated models for compressibility and rarefaction, showing effect of transonic bump on quasi nexus.

at supersonic and hypersonic conditions. At high Reynolds numbers, the results indicated that the drag crisis was delayed to higher Reynolds numbers, indicating $Re_{p,\mathrm{crit}} > 10^6$ for supersonic conditions.

In addition, new Navier–Stokes and DSMC simulations were conducted to investigate the behavior of the drag coefficient at Reynolds numbers near 45. The overall combination of the supersonic and hypersonic regimes provided by the data (and predicted by the present model) are shown in Fig. 11, where the compression-dominated region ($Re_p < 30$) yields an increase in C_D as M_p increases; whereas the rarefaction-dominated ($Re_p > 60$) yields a decrease in C_D as M_p increases. In between these regimes, there is a quasi nexus with a weak transonic bump occurring that bridges the rarefaction-dominated regime and the compression-dominated regime. The present simulations are the first to quantitatively describe this transonic bump for this Reynolds number, but the wide spread of experimental data indicates further work is needed to better understand and model this quasi nexus.

Empirical models were also developed, taking advantage of the comprehensive experimental dataset, new simulation results, and an improved understanding of the quasi-nexus behavior, especially for transonic conditions in the compression-dominated region. The new empirical models are as much as twice more accurate than previous models and served to provide an overall description of the drag coefficient for a wide range of Mach, Knudsen, and Reynolds numbers. However, additional simulations and experiments are recommended to better understand the fluid physics and the drag coefficient in the quasi-nexus regime, as well as in the influence of Mach number in the subsonic limit creeping flow for rarefied conditions.

Acknowledgments

The authors would like to thank Mr. Garret Hanrahan for preparing the Figures 6 and 7 and developing the associated empirical model, while as an undergraduate student at the University of Virginia.

References

[1] Connolly, B., and Loth, E., "Simulations of Ash and Sand Impact on a Hypersonic Forebody," *AIAA International Space Planes and Hypersonic Systems and Technologies Conference*, AIAA Paper 2020-2406, March 2020. https://doi.org/10.2514/6.2020-2406

[2] Crowe, C. T., "Drag Coefficient of Particles in a Rocket Nozzle," *AIAA Journal*, Vol. 5, No. 5, 1967, pp. 1021–1022. https://doi.org/10.2514/3.4119

[3] Loth, E., and Sivier, S., "Dusty Detonation Simulations with Adaptive Unstructured Finite Elements," *AIAA Journal*, Vol. 35, No. 6, 1997, pp. 1018–1024. https://doi.org/10.2514/2.189

[4] Li, X., and Bai, B., "Motion of Submicron Particles in Supersonic Laminar Boundary Layers," *AIAA Journal*, Vol. 53, No. 4, 2015, pp. 1037–1047. https://doi.org/10.2514/1.J053364

[5] Jodoin, B., "Cold Spray Nozzle Mach Number Limitation," *Journal of Thermal Spray Technology*, Vol. 11, Dec. 2002, pp. 496–507. https://doi.org/10.1361/105996302770348628

[6] Clift, R., and Gauvin, W. H., "The Motion of Entrained Particles in Gas Streams," *Canadian Journal of Chemical Engineering*, Vol. 49, No. 4, Aug. 1971, pp. 439–448.

[7] Aerosty, J., "Sphere Drag on a Low Density Flow," NASA TR HE-150-192, 1962.

[8] Bailey, A. B., and Hiatt, J., "Sphere Drag Coefficients for a Broad Range of Mach and Reynolds Numbers," *AIAA Journal*, Vol. 10, No. 11, 1972, pp. 1436–1440. https://doi.org/10.2514/3.50387

[9] Phillips, W. F., "Drag on a Small Sphere Moving Through a Gas," *Physics of Fluids*, Vol. 18, 1975, pp. 1089–1093.

[10] Basset, A. B., "On the Motion of a Sphere in a Viscous Liquid," *Philosophical Transactions of the Royal Society of London, Series A: Mathematical and Physical Sciences*, Vol. 179A, Jan. 1888, pp. 43–63.

[11] Epstein, P. S., "Zur Theorie des Radiometers," *Zeitschrift für Physik*, Vol. 54, July 1929, pp. 537–563.

[12] Millikan, R. A., "Coefficients of Slip in Gasses and the Law of Reflection of Molecules from the Surface of Solids and Liquids," *Physical Reviews*, Vol. 21, March 1923, pp. 217–238. https://doi.org/10.1103/PhysRev.21.217

[13] Parmar, M., Haselbacher, A., and Balachandar, S., "Equation of Motion for a Sphere in Non-Uniform Compressible Flows," *Journal of Fluid Mechanics*, Vol. 699, April 2012, pp. 352–375. https://doi.org/10.1017/jfm.2012.109

[14] Talbot, L., Cheng, R. K., Schefer, R. W., and Willis, D. R., "Thermophoresis of Particles in a Heated Boundary Layer," *Journal of Fluid Mechanics*, Vol. 101, No. 4, 1980, pp. 737–758. https://doi.org/10.1017/S0022112080001905

[15] Brock, J. R., "On the Theory of Thermal Forces Acting on Aerosol Particles," *Journal of Colloid Science*, Vol. 17, No. 8, Oct. 1962, pp. 768–780. https://doi.org/10.1016/0095-8522(62)90051-X

[16] Loth, E., "Drag of Non-Spherical Solid Particles of Regular and Irregular Shape," *Powder Technology*, Vol. 182, No. 3, March 2008, pp. 342–353. https://doi.org/10.1016/j.powtec.2007.06.001

[17] Loth, E., "Review: Lift of a Spherical Particle Subject to Vorticity and/or Spin," *AIAA Journal*, Vol. 46, No. 4, 2008, pp. 801–809. https://doi.org/10.2514/1.29159

[18] Michaelides, E. E., "High Reynolds Number Flows," *Particles, Bubbles, and Drops*, World Scientific, Singapore, 2006, pp. 107–156. https://doi.org/10.1142/9789812774316_0004

[19] Parmar, M. K., Haselbacher, A., and Balachandar, S., "Modeling of the Unsteady Force for Shock-Particle Interaction," *Shock Waves*, Vol. 19, May 2009, pp. 317–329. https://doi.org/10.1007/s00193-009-0206-x
[20] Parmar, M., Haselbacher, A., and Balachandar, S., "Generalized Basset-Boussinesq-Oseen Equation for Unsteady Forces on a Sphere in a Compressible Flow," *Physical Review Letters*, Vol. 106, Feb. 2011, Paper 084501. https://doi.org/10.1103/PhysRevLett.106.084501
[21] Cunningham, E., "On the Velocity of Steady Fall of Spherical Particles Through Fluid Medium," *Proceedings of the Royal Society of London, Series A: Mathematical and Physical Sciences*, Vol. 83, No. 563, 1910, pp. 302–323. https://doi.org/10.1098/rspa.1910.0018
[22] Bird, G. A., "Approach to Transitional Equilibrium in a Rigid Sphere Gas," *Physics of Fluids*, Vol. 6, No. 10, 1963, Paper 1518. https://doi.org/10.1063/1.1710976
[23] Bird, G. A., *Molecular Gas Dynamics and the Direct Simulation of Gas Flows*, 2nd Rev. ed., Oxford Univ. Press, New York, 1994.
[24] Loth, E., "Compressibility and Rarefaction Effects on Drag of a Spherical Particle," *AIAA Journal*, Vol. 45, No. 9, 2008, pp. 2219–2228. https://doi.org/10.2514/1.28943
[25] Parmar, M., Haselbacher, A., and Balachandar, S., "Improved Drag Correlation for Spheres and Application to Shock-Tube Experiments," *AIAA Journal*, Vol. 48, No. 6, 2010, pp. 1273–1276. https://doi.org/10.2514/1.J050161
[26] Jacobs, E. N., "Sphere Drag Tests in the Variable Density Wind Tunnel," NACA TN-312, 1929.
[27] Roos, F. W., and Willmarth, W. W., "Some Experimental Results on Sphere and Disk Drag," *AIAA Journal*, Vol. 9, No. 2, 1971, pp. 285–291. https://doi.org/10.2514/3.6164
[28] Short, B. J., "Dynamic Flight Behavior of a Ballasted Sphere at Mach Numbers from 0.4 to 14.5," NASA TN D-4198, 1967.
[29] Spearman, M. L., and Braswell, D. O., "Aerodynamics of a Sphere and an Oblate Spheroid for Mach Numbers from 0.6 to 10.5 Including Some Effects of Test Conditions," NASA TM-109016, 1993.
[30] Theofanous, T. G., Mitkin, V., and Chang, C., "Shock Dispersal of Dilute Particle Clouds," *Journal of Fluid Mechanics*, Vol. 841, Feb. 2018, pp. 732–745. https://doi.org/10.1017/jfm.2018.110
[31] Nagata, T., Nonomura, T., Tkahasahi, S., Mizuno, Y., and Fukuda, K., "Investigation on Subsonic to Supersonic Flow Around a Sphere at Low Reynolds Number of Between 50 and 300 by Direct Numerical Simulation," *Physics of Fluids*, Vol. 28, No. 5, 2016, Paper 056101. https://doi.org/10.1063/1.4947244
[32] Nagata, T., Nonomura, T., Takahashi, S., and Fukuda, K., "Direct Numerical Simulation of Subsonic, Transonic and Supersonic Flow over an Isolated Sphere up to a Reynolds Number of 1000," *Journal of Fluid Mechanics*, Vol. 904, Oct. 2020, Paper A36. https://doi.org/10.1017/jfm.2020.629
[33] Gallis, M. A., Torczynski, J. R., Plimpton, S. J., Rader, D. J., and Koehler, T., "Direct Simulation Monte Carlo: The Quest for Speed," *AIP Conference Proceedings*, Vol. 1628, No. 1, 2014, Paper 27. https://doi.org/10.1063/1.4902571
[34] Bird, G. A., *Molecular Gas Dynamics and the Direct Simulation of Gas Flows*, Oxford Univ. Press, New York, 1994.
[35] Nonomura, T., Terakado, D., Abe, Y., and Fujii, K., "A New Technique for Freestream Preservation of Finite-Difference WENO on Curvilinear Grid," *Computers and Fluids*, Vol. 107, Jan. 2015, pp. 242–255. https://doi.org/10.1016/j.compfluid.2014.09.025
[36] Pirozzoli, S., "Stabilized Non-Dissipative Approximations of Euler Equations in Generalized Curvilinear Coordinates," *Journal of Computational Physics*, Vol. 230, No. 8, 2011, pp. 2997–3014. https://doi.org/10.1016/j.jcp.2011.01.001
[37] Gottlieb, S., and Shu, C.-W., "Total Variation Diminishing Runge–Kutta Schemes," *Mathematics of Computation*, Vol. 67, No. 221, 1998, pp. 73–85.
[38] Bailey, A. B., and Starr, R. F., "Sphere Drag at Transonic Speeds and High Reynolds Numbers," *AIAA Journal*, Vol. 14, No. 11, 1976, Paper 1631. https://doi.org/10.2514/3.7262
[39] Carros, R. J., "Effect of Mach Number on Boundary-Layer Transition in the Presence of Pressure Rise and Surface Roughness on an Ogive-Cylinder Body with Cold Wall Conditions," NACA R&M A56B15, 1956.
[40] Risius, S., and Costantini, M., "Unit Reynolds Number, Mach Number and Pressure Gradient Effects on Laminar–Turbulent Transition in Two-Dimensional Boundary Layers," *Experiments in Fluids*, Vol. 59, May 2018, Paper 86. https://doi.org/10.1007/s00348-018-2538-8
[41] Millikan, R. A., "The Isolation of an Ion, A Precision Measurement of Its Charge, and the Correction of Stokes's Law," *Physical Review*, Vol. 32, April 1911, p. 349. https://doi.org/10.1103/PhysRevSeriesI.32.349
[42] Benson, C. M., Levin, D. A., Zhing, J., Gimelshein, S. F., and Montaser, A., "Kinetic Model for Simulation of Aerosol Droplets in High-Temperature Environments," *Journal of Thermophysics and Heat Transfer*, Vol. 18, Jan. 2004, pp. 122–134. https://doi.org/10.2514/1.1264
[43] Stadler, J. R., and Zurick, V. J., "Theoretical Aerodynamic Characteristics of Bodies in Free-Molecule Flow Field," NACA TN 2423, 1951, p. 12.
[44] Schaaf, S. A., and Chambré, P. L., "The Flow of Rarefied Gases," *Section of Fundamentals of Gas Dynamics*, edited by H. W. Emmons, Princeton Univ. Press, Princeton, NJ, 1958.
[45] White, F., *Viscous Fluid Flow*, 3rd ed., McGraw–Hill, New York, 2011.
[46] Hoerner, S. F., *Fluid Dynamic Drag: Practical Information on Aerodynamic Drag and Hydrodynamic Resistance*, 2nd ed., Hoerner Fluid Dynamics, Brick Town, NJ, 1965.
[47] Van Dyke, M., *An Album of Fluid Motion*, 14th ed., Parabolic Press, Stanford, CA, 1982.
[48] Wegener, P. P., and Ashkenas, H., "Wind Tunnel Measurements of Sphere Drag at Supersonic Speeds and Low Reynolds Numbers," *Journal of Fluid Mechanics*, Vol. 10, No. 4, 2006, pp. 550–560. https://doi.org/10.1017/S0022112061000354
[49] Carlson, D. J., and Hoglund, R. F., "Particle Drag and Heat Transfer in Rocket Nozzles," *AIAA Journal*, Vol. 2, No. 11, 1964, pp. 1980–1984. https://doi.org/10.2514/3.2714
[50] Overell, P., "Numerical Simulation of Rarefied Flow over a Hemispherical Body Using Direct Simulation Monte Carlo Method and Investigation of Scaling Parameters to Define the Flow," B.S. Engineering Thesis, School of Engineering, Univ. of Queensland, Brisbane, QLD, Australia, 2006.
[51] Mishin, G. I., "Experimental Investigation of the Flight of a Sphere in Weakly Ionized Air," AIAA Paper 1997-2298, June 1997.
[52] Goin, K. L., and Lawrence, W. R., "Subsonic Drag of Spheres at Reynolds Numbers from 200 to 10,000," *AIAA Journal*, Vol. 6, No. 5, 1964, pp. 961–962. https://doi.org/10.2514/3.4648
[53] Macrossan, M. N., "Scaling Parameters in Rarefied Flow and the Breakdown of the Navier–Stokes Equations," Dept. of Mechanical Engineering, Univ. of Queensland TR 2004/09, Brisbane, QLD, Australia, 2004.

D. S. Stewart
Associate Editor